interaction, the Reynolds stress model that imposes both the convective and diffusive effects of Reynolds stresses does produce the best agreement with experimental data among these turbulence models, although both the Reynolds stress model and algebraic stress model give similar accuracy in predicting the shock location.

Figure 2 shows the comparisons of the velocity profiles in the postshock separated region and the recovering zone following reattachment by various turbulence models. The differences especially near the wall region show the ability of these models to capture the separation process. The Reynolds stress model predicts best the start of separation and the separation process, however, the broad recirculation bubble also implies the underestimation of the velocity during flow redevelopment and an insufficient rate of recovery. The k-ϵ two-equation model reveals an insufficient level of interaction and thus fails to capture the onset of separation and gives a smaller recirculation region, but the smaller recirculating zone gives the "appearing good" agreement of the velocity profiles with measurement in the redeveloping region. The ASM/k-ϵ model induces separation earlier than the eddy viscosity model but slightly later than the Reynolds stress model. Also, the Reynolds stress model has the greatest sensitivity to the shock, the ASM/k-ϵ two-layer model exhibits a little less sensitivity to the shock, and the k-ϵ two-equation model gives the least sensitivity of the boundary layer to the shock.

It is expected that the shock and the velocity gradients in the separated region can elevate the streamwise turbulent stress by the contribution of streamwise strain to turbulent production, but the contribution is somewhat overestimated by these turbulence models when the computed profiles are compared with measured profiles (Fig. 3a). However, the predicted turbulent shear stress distribution at selected streamwise stations agree with measurement in terms of magnitudes with a little mismatch of peak locations (Fig. 3b). It also shows that both the Reynolds stress model and the ASM/k-ϵ two-layer model, which include the anisotropic effects of turbulent properties, obtain better predictions of the Reynolds shear stress than the eddy-viscosity, two-equation k-ϵ turbulence model.

The convergence and stability of the computational method is another concern of the present study. When the computations were performed on the CONVEX 3460, the computational efficiencies for the Reynolds stress model, ASM/k-ϵ model, and k-ϵ model are 4.13×10^{-4}, 3.90×10^{-4}, and 3.67×10^{-4} CPU s/grid/iteration, respectively. The L_2 residuals can be reduced to 3×10^{-9} after about 4000 iteration time steps which correspond to a total CPU time of about 5–6 h. It is noted that the computation is started from the freestream initial conditions and no prerun or other special treatment is necessary for initial guess of flowfield. Also, the computations are performed with the higher order closure turbulence models from the first time step, which is different from other investigations. Other computations usually start with an algebraic turbulence model until a nearly converged solution is obtained, and then continue with the higher order closure turbulence model.

V. Conclusions

Conclusions regarding the present study can be made as follows:

1) The Reynolds stress model has the best performance in predicting the onset of the separation process, mean velocity profiles, and turbulent normal and shear stresses in the separated region for the test case. The Reynolds stress model does predict the mean flowfield very well but needs further improvement in predicting turbulent quantities in the regions near the shock or expansion wave. All three turbulence models underestimate the recovery rate of mean flowfields in the redeveloping region.

2) The numerical method can perform the computation for compressible, complex turbulent, separated flow with high accuracy and a fast convergence rate.

Acknowledgment

The authors want to thank the National Science Council of Republic of China for its support under Contract NSC-82-0413-E-007-109.

References

[1]Johnson, D. A., Horstman, C. C., and Bachalo, W. D., "Comparison Between Experiment and Prediction for a Transonic Turbulent Separated Flow," *AIAA Journal*, Vol. 20, No. 6, 1982, pp. 737–744.

[2]Chuang, C. C., and Chieng, C. C., "Transonic Turbulent Separated Flow Predictions Using a Two-Layer Turbulent Model," *AIAA Journal*, Vol. 31, No. 5, 1993, pp. 816, 817; also AIAA Paper 92-0518, Jan. 1992.

[3]Launder, B. E., "Second-Moment Closure: Present and Future?" *International Journal of Heat and Fluid Flow*, Vol. 10, No. 4, 1989, pp. 282–299.

[4]Chien, K. Y., "Prediction of Channel and Boundary-Layer Flows with a Low-Reynolds-Number Turbulence Model," *AIAA Journal*, Vol. 20, No. 1, 1982, pp. 33–38.

[5]Shima, N., "A Reynolds-Stress Model for Near-Wall and Low-Reynolds-Number Regions," *Journal of Fluids Engineering*, Vol. 110, March 1988, pp. 38–44.

[6]Yee, H. C., and Harten, A., "Implicit TVD Scheme for Hyperbolic Conservation Laws in Curvilinear Coordinates," AIAA Paper 85-1513, July 1985.

[7]Van Der Vorst, H. A., "Bi-CGSTAB: A Fast and Smoothly Converging Variant of Bi-CG for the Solution of Nonsymmetric Linear Systems," *SIAM Journal of Scientific and Statistical Computing*, Vol. 13, No. 2, 1992, pp. 631–644.

[8]Lin, H., Yang, D. Y., and Chieng, C. C., "Variant Bi-Conjugate Gradient Methods for Compressible Navier-Stokes Solver with a Two-Equation Model of Turbulence," AIAA Paper 93-3316, July 1993.

[9]Bachalo, W. D., and Johnson, D. A., "Transonic, Turbulent Boundary-Layer Separation Generated on an Axisymmetric Flow Model," *AIAA Journal*, Vol. 24, No. 3, 1986, pp. 437–443.

Effect of Isotropy of Actuation Strains for a Plate with a Hole

Mohammed H. Kadivar,* K. Pradeep Sensharma,† and Raphael T. Haftka‡
Virginia Polytechnic Institute and State University, Blacksburg, Virginia 24061

Introduction

FOR a plate with a hole subject to uniform tension at its ends, there will be stress concentration around the hole. Shape memory alloys and piezoelectric materials can be used as induced strain elements to reduce stresses in the regions of stress concentration by applying energy, usually electric current. Sensharma et al.[1] showed that when isotropic actuation strains are applied in a ring centered at the hole, the stresses will not change in the interior of the ring. They also found numerically that when the actuation strains are anisotropic, the stresses in the interior of the ring will change. The objective of this work is to confirm analytically these results.

General Equations

For an isotropic plate subjected to actuation strains in the radial ε_{ir} and tangential $\varepsilon_{i\theta}$ directions, Hooke's law may be written as

$$\varepsilon_r = \frac{1}{E}(\sigma_r - \nu\sigma_\theta) + \varepsilon_{ir}$$
$$\varepsilon_\theta = \frac{1}{E}(\sigma_\theta - \nu\sigma_r) + \varepsilon_{i\theta} \quad (1)$$

Received March 18, 1993; revision received Feb. 10, 1994; accepted for publication Feb. 21, 1994.

*Visiting Professor, Mechanical Engineering Department; currently Associate Professor, Engineering School, Shiraz University, Shiraz, Iran.

†Graduate Research Assistant, Department of Aerospace and Ocean Engineering.

‡Christopher C. Kraft Professor, Department of Aerospace and Ocean Engineering. Associate Fellow AIAA.

We assume that constant actuation strains are applied in a ring $R_1 \le r \le R_2$ (see Fig. 1) leading to axisymmetric response. The equation of equilibrium in the radial direction is then

$$\sigma_\theta = \sigma_r + r\frac{d\sigma_r}{dr} = \frac{d(r\sigma_r)}{dr} \tag{2}$$

The strain displacements relations are

$$\varepsilon_r = \frac{du}{dr}, \qquad \varepsilon_\theta = \frac{u}{r} \tag{3}$$

so that

$$\varepsilon_r = \frac{d}{dr}(r\varepsilon_\theta) \tag{4}$$

Substituting Eq. (1) into Eq. (4) using Eq. (2), assuming that E is constant, and simplifying, we get

$$r\frac{d}{dr}\left[\frac{1}{r}\frac{d}{dr}(r^2\sigma_r)\right] = -Er\frac{d\varepsilon_{i\theta}}{dr} - E(\varepsilon_{i\theta} - \varepsilon_{ir}) \tag{5}$$

Integrating Eq. (5), we obtain

$$\sigma_r = -\frac{E}{r^2}\int \varepsilon_{i\theta} r_1\, dr_1 - \frac{E}{r^2}\iint r_2(\varepsilon_{i\theta} - \varepsilon_{ir})\frac{1}{r_1}\, dr_1\, dr_2 + A + \frac{B}{r^2} \tag{6}$$

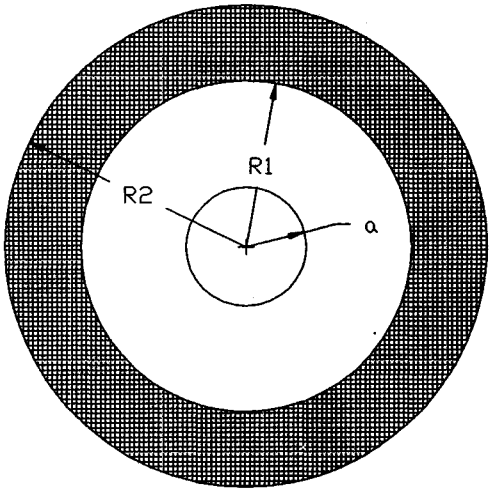

Fig. 1 Plate with hole geometry.

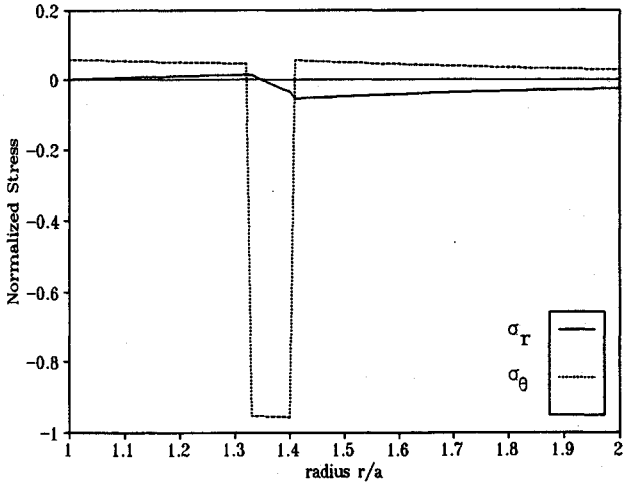

Fig. 2 Normalized stresses $\sigma/E\varepsilon_{i\theta}$ in plate when radial actuation strain is zero and $\varepsilon_{i\theta}$ is applied for $1.33 \le r/a \le 1.41$.

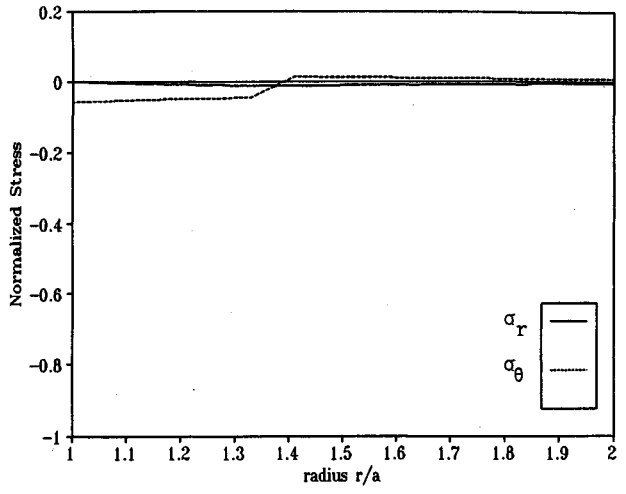

Fig. 3 Normalized stresses $\sigma/E\varepsilon_{ir}$ when tangential actuation strain is zero and ε_{ir} is applied for $1.33 \le r/a \le 1.41$.

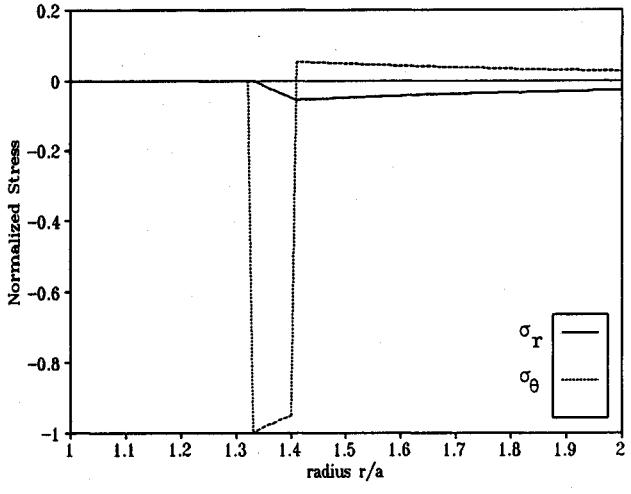

Fig. 4 Normalized stresses $\sigma/E\varepsilon_{ir}$ when isotropic actuation strains ($\varepsilon_{ir} = \varepsilon_{i\theta}$) are applied for $1.33 \le r/a \le 1.41$.

where A and B are constants that are found from the boundary conditions. We assume that the radius of the hole is small compared with the plate dimensions so that the plate may be treated as infinitely large. Then the boundary conditions are $\sigma_r(a) = 0$ and $\sigma_r \to 0$ as $r \to \infty$, and when these conditions are applied in Eq. (6), σ_r becomes

$$\sigma_r = -\frac{E}{r^2}\int_a^r \varepsilon_{i\theta} r_1\, dr_1 - \frac{E}{r^2}\int_a^r\int_a^{r_2} r_2(\varepsilon_{i\theta} - \varepsilon_{ir})\frac{1}{r_1}\, dr_1\, dr_2$$

$$+\frac{E}{2}\int_{R_1}^{R_2}(\varepsilon_{i\theta} - \varepsilon_{ir})\frac{1}{r_1}\, dr_1 - \frac{a^2}{2r^2}E\int_{R_1}^{R_2}(\varepsilon_{i\theta} - \varepsilon_{ir})\frac{1}{r_1}\, dr_1 \tag{7}$$

By substituting the value of σ_r from Eq. (7) into Eq. (2), one finds the tangential stress as

$$\sigma_\theta = \frac{E}{r^2}\int_a^r \varepsilon_{i\theta} r_1\, dr_1 + \frac{E}{r^2}\int_a^r\int_a^{r_2} r_2(\varepsilon_{i\theta} - \varepsilon_{ir})\frac{1}{r_1}\, dr_1\, dr_2 - E\varepsilon_{i\theta}$$

$$-E\int_a^r(\varepsilon_{i\theta} - \varepsilon_{ir})\frac{1}{r_1}\, dr_1 + \frac{E}{2}\int_{R_1}^{R_2}(\varepsilon_{i\theta} - \varepsilon_{ir})\frac{1}{r_1}\, dr_1$$

$$+\frac{a^2}{2r^2}E\int_{R_1}^{R_2}(\varepsilon_{i\theta} - \varepsilon_{ir})\frac{1}{r_1}\, dr_1 \tag{8}$$

Consider now the case of constant actuation strains $\varepsilon_{i\theta}$ and ε_{ir}, applied only for a ring $R_1 \le r \le R_2$. We can specialize the equations for σ_r and σ_θ to three regions, as follows:

For $a \le r \le R_1$:

$$\sigma_r = \frac{E(\varepsilon_{i\theta} - \varepsilon_{ir})}{2}\left(1 - \frac{a^2}{r^2}\right)\ell_n\left(\frac{R_2}{R_1}\right)$$

$$\sigma_\theta = \frac{E(\varepsilon_{i\theta} - \varepsilon_{ir})}{2}\left(1 + \frac{a^2}{r^2}\right)\ell_n\left(\frac{R_2}{R_1}\right) \tag{9}$$

For $R_1 \le r \le R_2$:

$$\sigma_r = -\frac{E\varepsilon_{i\theta}}{2}\left(1 - \frac{R_1^2}{r^2}\right) - \frac{E(\varepsilon_{i\theta} - \varepsilon_{ir})}{2}\left[\ell_n\left(\frac{r}{R_1}\right) - \frac{1}{2} + \frac{R_1^2}{2r^2}\right]$$

$$+ \frac{E(\varepsilon_{i\theta} - \varepsilon_{ir})}{2}\left(1 - \frac{a^2}{r^2}\right)\ell_n\frac{R_2}{R_1} \tag{10}$$

$$\sigma_\theta = \frac{E\varepsilon_{i\theta}}{2}\left(1 - \frac{R_1^2}{r^2}\right) - \frac{E(\varepsilon_{i\theta} - \varepsilon_{ir})}{2}\left[\ell_n\left(\frac{r}{R_1}\right) + \frac{1}{2} - \frac{R_1^2}{2r^2}\right]$$

$$+ \frac{E(\varepsilon_{i\theta} - \varepsilon_{ir})}{2}\left(1 + \frac{a^2}{r^2}\right)\ell_n\left(\frac{R_2}{R_1}\right) - E\varepsilon_{i\theta}$$

For $r \ge R_2$:

$$\sigma_r = -\frac{E\varepsilon_{i\theta}}{2r^2}(R_2^2 - R_1^2) - \frac{E(\varepsilon_{i\theta} - \varepsilon_{ir})}{2}\frac{a^2}{r^2}\ell_n\left(\frac{R_2}{R_1}\right)$$

$$+ \frac{E(\varepsilon_{i\theta} - \varepsilon_{ir})}{4r^2}(R_2^2 - R_1^2)$$

$$\sigma_\theta = \frac{E\varepsilon_{i\theta}}{2r^2}(R_2^2 - R_1^2) + \frac{E(\varepsilon_{i\theta} - \varepsilon_{ir})}{2}\frac{a^2}{r^2}\ell_n\left(\frac{R_2}{R_1}\right) \tag{11}$$

$$- \frac{E(\varepsilon_{i\theta} - \varepsilon_{ir})}{4r^2}(R_2^2 - R_1^2)$$

As was found numerically in Ref. 1, there are nonzero stresses in the interior region, Eq. (9), unless $\varepsilon_{ir} = \varepsilon_{i\theta}$. Figure 2 shows the stresses when $\varepsilon_{ir} = 0$. The radial stress is very small in comparison with the tangential stress, especially in the area where the actuation strain is applied. When the actuation strain in the tangential direction is zero (Fig. 3), both the tangential and radial stresses are small in comparison with the preceding case. For isotropic actuation strains (Fig. 4), there is no effect at all on the interior of the region where actuation strains are applied. In the application ring, the tangential stress is high, and outside of the ring, the tangential stress is positive, whereas the radial stress is negative, and their values are very small in comparison with the value of tangential stress in the ring.

Acknowledgments

This work was supported by NASA Grant NAG-1-168 and U.S. Army Research Office Grant DAAL03-92-G-0180.

References

[1]Sensharma, P. K., Palantera, M. J., and Haftka, R. T., "Stress Reduction in an Isotropic Plate with a Hole by Applied Induced Strains," *Proceedings of the AIAA/ASME/ASCE/AHS/ASC 33rd Structures, Structural Dynamics, and Materials Conference* (Dallas, TX), Pt. 2, AIAA, Washington, DC, 1992, pp. 905–913 (AIAA Paper 92-2525).